Molecular Insights into the Influence of Ions on Water Structure. I. Alkali Metal Ions in Solution

Roya Savoj,[†] Henry Agnew,[†] Ruihan Zhou,[†] and Francesco Paesani[*,†,‡,¶,§]

[†]*Department of Chemistry and Biochemistry, University of California San Diego, La Jolla, California 92093, United States*

[‡]*Materials Science and Engineering, University of California San Diego, La Jolla, California 92093, United States*

[¶]*Halicioğlu Data Science Institute, University of California, San Diego La Jolla, California 92093, United States*

[§]*San Diego Supercomputer Center, University of California San Diego, La Jolla, California 92093, United States*

E-mail: fpaesani@ucsd.edu

Abstract

In this study, we explore the impact of alkali metal ions (Li^+, Na^+, K^+, Rb^+, and Cs^+) on the hydration structure of water using molecular dynamics simulations carried out with the MB-nrg potential energy functions (PEFs). Our analyses include radial distribution functions, coordination numbers, dipole moments, and infrared spectra of water molecules, calculated as a function of solvation shells. The results collectively indicate a highly local influence of all the alkali metal ions on the hydrogen-bond network established by the surrounding water molecules, with the smallest and most densely charged Li^+ ion exerting the most pronounced effect. Remarkably, the MB-nrg PEFs demonstrate excellent agreement with available experimental data for the position and size of the first solvation shells, underscoring their potential as predictive models for realistic simulations of ionic aqueous solutions across various thermodynamic conditions and environments.

INTRODUCTION

The investigation of the hydration properties of ions in aqueous solutions has been a subject of scientific curiosity and intensive research for nearly a century.[1] Initial interest was stimulated by understanding chemical reactions in aqueous media, which requires a comprehensive knowledge of ion hydration in terms of both energetics and formation of water microstructures around ions.[2] The study of ion hydration has increasingly gained more significance across a wide spectrum of scientific domains, encompassing biological research, environmental science, and energy storage systems, where a molecular-level understanding of how ions behave plays a central role.[3]

In this context, the study of alkali metal ions (Li^+, Na^+, K^+, Rb^+, and Cs^+) holds significant importance in both biological[4] and industrial realms.[5] The relevance of Li^+ ions in today's society cannot be overemphasized given the key role that they play in rechargeable batteries.[6] Na^+ and K^+ ions are abundant in living systems, mediating fundamental processes

such as nerve signal transmission and cellular function regulation through mechanisms like the sodium-potassium pump.[7] While the role of Rb^+ is more limited, radioactive ^{137}Cs atoms are common byproducts of nuclear reactors, posing a significant concern given their relatively long half-life of about 30 years and their high solubility in water as Cs^+ ions.[8] Moreover, a precise molecular-level understanding of the hydration properties of alkali-metal ions has far-reaching implications for various technological applications, ranging from water desalination to implantable electrical power generation.

The Hofmeister's series was the first attempt to conceptualize ion's effects on the properties of aqueous solutions.[9,10] Based on these findings, Gurney introduced the concept of "structure makers" (or "kosmotropes") and "structure breakers" (or "chaotropes") to describe ions with strong and weak hydration, respectively.[11] According to this classification, small, highly charged ions are considered "structure makers" because they reinforce the water's hydrogen-bond network, whereas large, monovalent ions are considered "structure breakers" because they disrupt the water's hydrogen-bond network, resulting in a more disordered liquid structure. This classification suggests that "structure makers" can influence the structural properties of aqueous solutions over long distances, leading to long-range ordering.[12]

Over the years, significant advancements have been made in both the sophistication of experimental techniques and the realism of theoretical and computational models to probe the behavior of hydrated alkali metal ions. Gas-phase clathrate-like structures with Cs^+ ions encaged within water hydrogen-bonded networks were first observed using a fast-flow reactor for cluster production under thermalized conditions.[13] Among possible clathrate-like structures, $Cs^+(H_2O)_{20}$ was found to exhibit remarkable stability. Diverse clathrate configurations were also identified for clusters of 18, 22, 24, 27, and 29 water molecules surrounding the Cs^+ ion. Subsequently, infrared predissociation (IRPD) spectra of $M^+(H_2O)_{4-7}$ clusters were reported using a triple-quadrupole mass spectrometer paired with an infrared (IR) laser.[14] Detailed analyses of the spectral features provided evidence of multiple photon absorption

processes as well as how water–water interactions begin to dominate as more water molecules are added to the clusters. In addition, the fragmentation processes were found to be mode specific, with free-OH and linear hydrogen-bonded OH stretching features being relatively unaffected by the loss channel, and cyclic- and bent-type hydrogen-bonded OH stretches displaying diminished cross sections. Using IRPD spectroscopy and blackbody infrared radiative dissociation (BIRD), clusters of K^+, Rb^+, and Cs^+ with 18 and 20 water molecules were found to have anomalously high abundances, providing support for the formation of clathrate structures .[15] Conversely, the presence of significant acceptor-donor bands in the IRPD spectra suggested different types of structures for Na^+, while Li^+ showed evidence of clathrate structures only for clusters with 20 water molecules.

Dielectric relaxation spectroscopy (DRS) measurements showed that the hydration numbers for alkali-metal fluorides did not follow a simple sequential trend, instead varying as CsF < NaF < RbF < KF, which was attributed to the differences in M^+–OH_2 bonding strength.[16] It was also found that the number of strongly bound water molecules around each alkali metal ion varies systematically with the charge density, following the order $Li^+ \gg Na^+ > K^+ > Rb^+ > Cs^+$. Interestingly, the same trend was also found for the number of moderately bound water molecules, except for Li^+ and Na^+, where the presence of strongly bound water molecules in the hydration shells reduces the possibility of further interactions with surrounding water molecules, leading to an absence of slow water around these ions. Large angle X-ray scattering (LAXS) and double difference infrared spectroscopy (DDIR) measurements showed that Na^+, K^+, Rb^+, and Cs^+ ions are weakly hydrated with a single shell of water molecules, while the smaller Li^+ ion is more strongly hydrated, likely showing a second hydration shell.[17] Except for lithium, the LAXS measurements also allowed for fairly accurate determination of the mean M^+–O distances, which were found to be 2.43(2), 2.81(1), 2.98(1) and 3.07(1) Å, for Na^+, K^+, Rb^+, and Cs^+, respectively, corresponding to coordination numbers of six, seven, eight, and eight. Based on the analyses of the LAXS and DDIR measurements, it was concluded that Li^+ is a structure maker, while K^+, Rb^+,

and Cs^+ are structure breakers. The role of Na^+ was less clear, suggesting a borderline behavior. Polarization-selective IR pump-probe spectroscopy and two-dimensional IR vibrational echo spectroscopy were used to probe the dynamics of the hydrogen-bond network in dilute HOD in H_2O/salt solutions.[18] It was found that the shift in the absorption frequency of the OD stretch becomes more pronounced as the size of the alkali-metal ion of the salt pair decreases. Liquid-jet X-ray photoelectron experiments found that Li^+ ions adsorb to the air-water interface, exhibiting "surfactant-like" behavior, while K^+ ions do not.[19] The difference in adsorption behavior of Li^+ and K^+ ions was attributed to the different resilience of their hydration shells.

On the theoretical/simulation side, early molecular dynamics (MD) simulations of small $Na^+(H_2O)_n$ clusters predicted that Na^+ resides in the interior of the clusters independently of whether pairwise additive or polarizable force fields were used to model the underlying molecular interactions.[20] Subsequent studies focused on improving the description of ion–water interactions through empirical parameterization of pairwise additive force fields. Refined models of Li^+, Na^+, K^+, Rb^+, and Cs^+ compatible with the TIP3P, TIP4PEW, and SPC/E water models were obtained by tuning the Coulombic and Lennard-Jones parameters to balance crystal and solution properties.[21] Along similar lines, improved pairwise parameterizations compatible with the OPC3, OPC, TIP3P-FB, and TIP4P-FB water models were introduced to describe monovalent ions in liquid water.[22] By adopting scaled charges to effectively account for electronic polarization, new pairwise parameters for alkali metal ions compatible with the TIP4P/2005 water model were shown to result in more accurate predictions of the density, viscosity, and structural properties of ionic solutions up to high concentrations.[23,24] Although using scaled charges led to an improved description of some properties of ionic aqueous solutions, it was also found that different sets of scaled charges are required to predict different structural, thermodynamic, and dynamical properties.[25] MD simulations using a polarizable force field accurately predicted the ion-oxygen distances within the first hydration shell of K^+ in water. These predictions were within 0.05-0.1 Å of

the values determined experimentally from extended X-ray absorption fine structure (EXAFS) spectra.[26] More accurate representations of ion–water interactions, including charge penetration, charge transfer, and geometry-dependent charge flux effects were introduced with the AMOEBA+ polarizable force field.[27] AMOEBA+ demonstrates improved accuracy in capturing a range of ion properties from gas phase to solution phase and crystals, providing energy components consistent with quantum-mechanical energy decomposition schemes.

Electronic structure calculations carried out for small ion–water clusters using density functional theory (DFT) indicated that, as the number of water molecules increases, molecular polarization is primarily influenced by water–water interactions rather than ion–water interactions.[28] Based on these results it was concluded that as the cluster size grows, the average dipole moment of all water molecules, including those in the first solvation shell, tends to match the average of a similarly sized cluster of pure water. Ab initio molecular dynamics (AIMD) simulations of aqueous solutions under physiological conditions found that Li^+, Na^+, and K^+ strongly coordinate with four water molecules, and revealed the presence of additional "loosely" coordinated water molecules, leading to hydration numbers of 5 and 6 for Na^+ and K^+, respectively.[29] Analyses of the self-diffusion coefficient and rotational correlation time of water calculated from AIMD simulations carried out with the HCTH density functional suggested that Li^+ ions act as structure makers, whereas K^+ ions are structure breakers, and Na^+ ions function as weak structure breakers.[30] AIMD simulations carried out with various van der Waals (LMKLL, DRSLL, DRSLL-PBE, DRSLL-optB88), dispersion-corrected (BLYP-D3), and conventional gradient-corrected (GGA-BLYP) density functionals found that incorporating dispersion forces enhances the accuracy in predicting the local hydration structure of both Na^+ and K^+ in solution, aligning the simulation results more closely with the experimental data.[31] Similar conclusions were reached from analogous AIMD simulations carried out with the revPBE functional including a van der Waals correction.[32] MD simulations carried out with a pairwise additive model as well as AIMD simulations carried out with the revPBE and BLYP density functionals were used to ex-

amine the hydration structure of aqueous Na^+.[33] Both revPBE and BLYP predicted Na–O distances longer by about 0.05 Å than the experimental value, with the difference increasing to 0.07 Å after including a dispersion correction. In contrast, a pairwise additive force field based on the SPC/E water model was found to predict the Na–O distance in good agreement with the experimental value, though the resulting Na–O peak in the EXAFS spectrum was overstructured compared to the experimental data. AIMD simulations carried out with density functionals belonging to different rungs across the Jacob's ladder of DFT approximations (i.e., revPBE and SCAN) as well as using the random phase approximation (RPA) were employed to model the hydration structure of Na^+ and K^+ in solution.[34] Comparisons with X-ray measurements showed that the SCAN functional accurately reproduces key structural details of the hydration structure around both ions, unlike revPBE-D3. However, it was also found that the SCAN density functional is less effective in describing bulk water compared to revPBE-D3, which is related to the interplay of functional-driven and density-driven errors in DFT models of aqueous systems.[35–38] The RPA simulations also showed some improvement in the description of the hydration structure of K^+ ions, but slow convergence precluded a more systematic comparison.

More recently, our group introduced the many-body energy (MB-nrg) theoretical and computational framework for data-driven many-body potential energy functions (PEFs) of generic molecules.[39–43] Building upon the accuracy of the MB-pol PEF,[44–48] which was shown to accurately predict the properties of water across the entire phase diagram,[49] from gas-phase clusters[50–52] to liquid water[53–58] and ice[59–62] phases, the MB-nrg PEF of a given molecular system is rigorously derived from the corresponding many-body expansion (MBE) of the system's energy. Within the MB-nrg framework, the MBE is calculated at the coupled cluster level of theory, including single, double, and perturbative triple excitations, i.e., CCSD(T), which is currently considered as the "gold standard" for chemical accuracy.[63,64] A series of MB-nrg PEFs developed for alkali metal ions was shown to accurately predict the structures, binding and interaction energies, and vibrational spectra of small $M^+(H_2O)_N$

clusters (M^+ = Li^+, Na^+, K^+, Rb^+, and Cs^+)[40,65–67] as well as the hydration structures of Na^+, K^+, and Cs^+ in solution.[68,69] The Supporting Information includes an overview of the main results obtained so far using the MB-pol and MB-nrg PEF, along with comparisons with common force fields and DFT models. This short overview aims to provide the reader with an up-to-date perspective on the performance of MB-pol and MB-nrg in the context of state-of-the-art computer simulations of various aqueous systems.

In this study, we employ the MB-nrg PEFs to characterize the hydration properties of the alkali metal ion series by linking structural, dynamical, and electrostatic properties to IR spectra calculated for individual solvation shells around each ion from MD simulations. Our analyses provide a unified molecular-level picture of the hydration structure of alkali metal ions in solution and allow for unambiguously assessing the effects of each ion on the surrounding water's hydrogen-bonding network.

METHODS

All MD simulations were performed using the Large-scale Atomic/Molecular Massively Parallel Simulator (LAMMPS)[70] interfaced with the MBX C++ library for data-driven many-body PEFs.[71,72] Each system consisted of 277 water molecules and 1 alkali metal ion (Li^+, Na^+, K^+, Rb^+ or Cs^+) placed in a cubic box in periodic boundary conditions, corresponding to a concentration of ∼0.2 M. The initial configurations were taken from previous simulations carried out with the MB-nrg PEFs,[68,69] which were further equilibrated for at least ∼150 ps in the isothermal-isobaric (NPT: constant number of atoms, pressure, and temperature) ensemble at 298 K and 1 atm. This was followed by a 400 ps-long simulation carried in the canonical (NVT: constant number of atoms, volume, and temperature) ensemble at 298 K and the equilibrated volume obtained from the NPT simulations. 30 distinct configurations were extracted at intervals of 10 ps from the last 300 ps of the NVT trajectories, which were then used to generate 30 independent 50 ps-long trajectories in the microcanonical ensem-

ble (NVE: constant number of atoms, volume, and energy). These 30 NVE trajectories were used to calculate all the structural and dynamical properties as well as infrared spectra reported in the following section. The temperature in the NPT and NVT simulations was controlled by a global Nosé-Hoover chain of three thermostats with a characteristic time of 1 ps.[73] The pressure in the NPT simulations was maintained by a global Nosé-Hoover chain of three barostats with a characteristic time of 2 ps.[73] The equations of motion were propagated with a time step of 0.5 fs according to the velocity-Verlet algorithm.[74] The non-bonded interactions were truncated at an atom-atom distance of 9.0 Å, and the long-range electrostatic interactions were treated using the particle mesh Ewald method as implemented in MBX.[71,72,75,76]

The dipole moments of the water molecules were calculated using the many-body MB-μ model.[53] MB-μ leverages the fast convergence of electrostatic properties within the MBE formalism[77] to rigorously express the total dipole moment of a molecular system (μ_{tot}) as a sum of individual n-body terms ($1 \leq n \leq N$), integrating explicit machine-learned 1-body (μ^{1B}) and 2-body (μ^{2B}) terms with an implicit N-body polarization term (μ^{NB}) describing all higher-body contributions:[53]

$$\mu_{\text{tot}}(1,\ldots,N) = \sum_{i=1}^{N} \mu^{\text{1B}}(i) + \sum_{i<j}^{N} \mu^{\text{2B}}(i,j) + \mu^{\text{NB}}(1,\ldots,N) \tag{1}$$

MB-μ accurately reproduces the dipole moment of generic water systems containing an arbitrary number of water molecules and has been used to calculate the infrared spectra of diverse water systems.[52–54,60,78–80] The IR spectra of water were calculated within a time-dependent formalism from the dipole-dipole time correlation function according to:

$$I_{IR}(\omega) \propto \int_{\infty}^{\infty} e^{-i\omega t} \langle \mu(0)\mu(t) \rangle dt \tag{2}$$

where μ is the total dipole moment of the water molecules represented by the MB-μ model along the NVE trajectory, and the angular brackets imply an ensemble average. It has

been shown that MB-μ quantitatively accounts for all many-body contributions to both the permanent and induced dipole moments of water and allows for accurate simulations of the IR spectra of water across different phases[52–56,60–62,78,81,82] and in different environments.[79,80,83–86] The simulated IR spectra were redshifted by 60 cm^{-1} and 175 cm^{-1} in the bending and stretching regions, respectively, to account for nuclear quantum effects in classical MD simulations of water carried out with the MB-pol PEF as discussed in Refs. 53–55,78. It should be emphasized that, apart from the red shifts mentioned above, quantum simulations of the infrared spectra of liquid water using centroid molecular dynamics (CMD)[87–93] yield vibrational lineshapes that are equivalent to those calculated from classical MD simulations.[55] This similarity justifies the use of classical MD in our study of the infrared spectra of water around alkali metal ions.

The residence time of the water molecules residing within the first solvation shell ($n_{1\mathrm{st}}$) of each alkali metal ion was calculated according to the algorithm introduced in Ref. 94,

$$n_{1\mathrm{st}}(t) = \frac{1}{N_t}\sum_{n=1}^{N_t}\sum_{j} P_j(t_n t; t^*) \tag{3}$$

Here, $P_j(t_n t; t^*)$ is equal to 1 if water molecule j lies within the first solvation shell at both time steps t_n and $t_n + t$, and does not leave the first solvation shell for a period longer than t^*. Under all other circumstances, $P_j(t_n t; t^*) = 0$. From Eq. 3, it follows that $n_{1\mathrm{st}}(0) = \langle n_{1\mathrm{st}} \rangle$, which is the average first-shell coordination number, whereas $n_{1\mathrm{st}}(t)$ corresponds to the number of molecules that reside initially within the first solvation shell and are still there after a time t has elapsed. The parameter t^* is introduced to account for molecules which only transiently leave the first coordination shell. Following Ref. 94, t^* was set to 2 ps in our analyses. Given the exponential decay of $n_{1\mathrm{st}}(t)$, the residence time of the water molecules in the first solvation shell of each alkali metal ion ($\tau_{1\mathrm{st}}$) was determined as the time t at which $C(t) = n_{1\mathrm{st}}(t)/\langle n_{1\mathrm{st}} \rangle = 1/e$, where $\langle n_{1\mathrm{st}} \rangle$ is the average first-shell coordination number. It should be noted that the actual value of the residence time $\tau_{1\mathrm{st}}$ shows some dependence on

the choice of t^* although the trend across the different ions is independent of it. In our analyses, we opted to use $t^* = 2$ ps in order to be consistent with the original definition.[94]

RESULTS

In Figure 1a, we present the M^+O radial distribution functions (RDFs) that directly map the spatial correlations between each alkali metal ion (M^+) and the oxygen atoms (O) of the surrounding water molecules. Complementing the RDFs, Figure 1b displays the corresponding M^+O cumulative distribution functions (CDFs) reporting the variation of the coordination number (n_{wat}) with respect to the distance from each alkali metal ion. Both RDFs and CDFs trace the gradual change in coordination environment, providing insights into the evolving nature of the hydration shells as one moves from Li^+ to Cs^+ ions. In this context, it should be noted that previous MD simulations carried out for Na^+, K^+, and Cs^+ with the corresponding MB-nrg PEFs provided quantitative agreement with the experimental EXAFS spectra, outperforming both force fields and DFT models.[68,69] Drawing from the systematic analyses of many-body interactions reported in Ref. 40, Figure 1a highlights a direct correlation between the ion–water interaction strength and the observed trends in both the position and the width of the first peak of the RDFs. This peak, representing

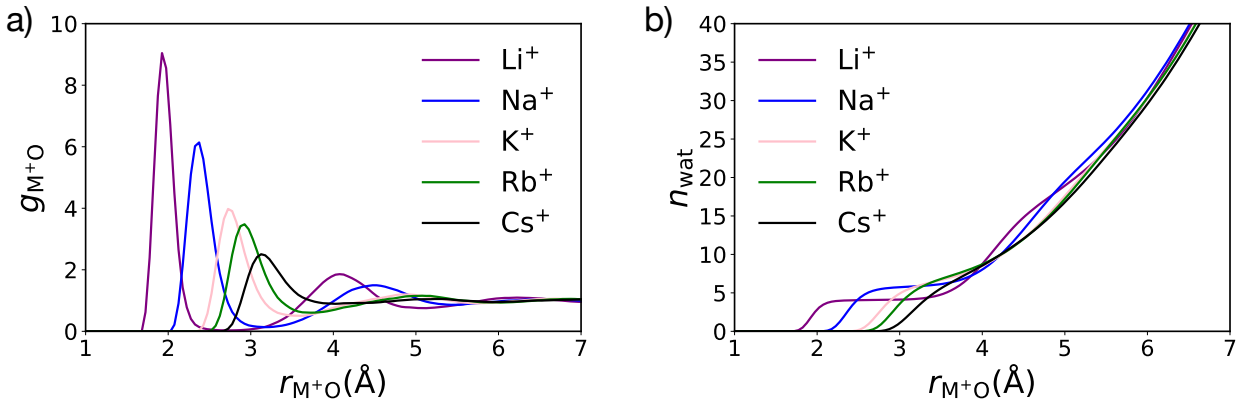

Figure 1: a) Ion–water radial distribution functions (g_{M^+O}) calculated from MD simulations carried out with the MB-nrg PEFs of each alkali metal ion (M^+). b) Coordination number (n_{wat}) as a function of the M^+–O distance (r_{M^+O}).

Table 1: Main characteristics of the first and second solvation shells around each alkali metal ion, as predicted by MD simulations with the MB-nrg PEFs. It includes the positions of the first-shell and second-shell peaks, the distances marking the end of these shells, and the corresponding coordination numbers. The experimental values are taken from Ref. 17 and references therein. The DFT values are taken from Refs. 29–32,34,95.

		Li^+	Na^+	K^+	Rb^+	Cs^+
Experiment	1st-shell peak position (Å)	1.90-2.17	2.34-2.50	2.65-2.97	2.83-3.05	2.95-3.21
	1st-shell coordination number	4-6	4-8	5.6-8.3	6-8	8-9
MB-nrg	1st-shell peak position (Å)	1.93	2.38	2.73	2.88	3.13
	1st-shell boundary (Å)	2.70	3.18	3.53	3.73	4.03
	1st-shell coordination number	4.1	5.8	6.7	7.6	8.7
	2nd-shell peak position (Å)	4.08	4.53	4.88	5.08	5.23
	2nd-shell boundary (Å)	5.13	5.48	5.73	5.83	5.92
	2nd-shell coordination number	19.9	24.5	26.6	27.9	28.4
DFT	1st-shell peak position (Å)	1.96-2.00	2.36-2.51	2.74-2.98	3.0-3.12	3.2
	1st-shell boundary (Å)	-	2.81-3.40	3.43-3.81	-	-
	1st-shell coordination number	4.0-4.2	5.0-6.09	5.5-7.5	6.95-7.77	7.07-7.69

water molecules in the first solvation shell of each alkali metal ion, not only moves to larger distances but also increases in width from Li^+ to Cs^+. The increasing ion's size leads to progressively less defined boundaries between the first and second solvation shells, resulting in a barely noticeable inflection point in the Cs^+ CDF. The changes in the RDFs and CDFs underscore the delicate balance between the underlying ion–water and water–water interactions, which directly correlate with the ion's and charge density.

Table 1 summarizes the main characteristics of the first and second solvation shells around each alkali metal ion calculated from the RDFs and CDFs of Figure 1. Specifically, besides the position of the first and second-shell peaks, Table 1 also lists the boundary distances defined the extent of these shells, alongside their respective coordination numbers. In all cases, the MB-nrg PEFs predict first-shell peak positions and coordination numbers in remarkable agreement with the available experimental data.[17] This level of agreement is particularly noteworthy given that the MB-nrg PEFs are rigorously derived from first principles to represent individual many-body contributions to the multidimensional Born-Oppenheimer energy

landscape. Therefore, contrary to pairwise-additive force fields that are empirically parameterized to reproduce a predetermined subset of experimental properties,[23–25] the MB-nrg PEFs do not have prior knowledge of any property of alkali metal ions in solution, which highlights the high degree of transferability and predictive capability of the MB-nrg PEFs. On the other hand, large variations in the AIMD predictions for both position and size of the first hydration shell are found for all the alkali metal ions. These differences highlight the challenges faced by current DFT models in accurately representing aqueous environments, particularly the delicate interplay and competition among different many-body effects in ion–water and water–water interactions,[39,40,65,96,97] which are directly related to functional-driven and density-driven errors.[35,37,98–101] In this context, it should be noted that recent developments have demonstrated that density-driven errors in the description of ion–water interactions can be partially corrected through a density-corrected DFT scheme.[36,38,102,103]

Figure 2 shows $C(t) = n_{1st}(t)/\langle n_{1st} \rangle$ as a function of time, whose decay directly reports on how long the water molecules remain in the first solvation shell of the different alkali metal ions. As discussed in the Methods section, in our analyses, the residence time, τ_{1st}, is defined

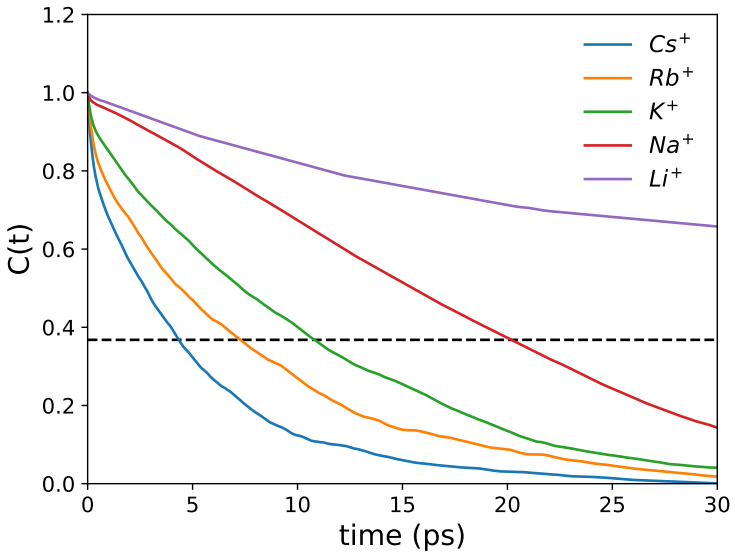

Figure 2: $C(t) = n_{1st}(t)/\langle n_{1st} \rangle$ as a function of time. The black dashed line corresponds to $C(t) = 1/e$. The residence time values for Li^+, Na^+, K^+, Rb^+, and Cs^+ are $>$ 100 ps, $\sim$20 ps, $\sim$11 ps, $\sim$7.5 ps, and $\sim$4.5 ps, respectively.

as time at which $C(t) = 1/e$, which is indicated as a black dashed line in Figure 2. The present MD simulations with the MB-nrg PEFs show a clear pattern, with the residence time progressively increasing as the strength of the underlying ion–water interactions increases.[40] Specifically, the data in Figure 2 indicate that the water molecules stay in the first solvation shell of Cs^+, which has the weakest interactions with water among the alkali metal ions, for only ∼4.5 ps. In contrast, for Li^+, which has the strongest interactions with water, the residence time extends beyond 100 ps. This trend of shorter residence times with weaker ion–water interaction strength is an important aspect of how ions influence their surrounding water molecules. The strong binding of Li^+ results in a more rigid first solvation shell, while larger ions like Cs^+ have a looser hold on the surrounding water molecules, allowing water molecules to diffuse in and out the first solvation shell over a significantly shorter time interval.

Further insights into the hydration properties of the alkali metal ions in solution are gained from the analysis of the dipole moment of water molecules residing in different solvation shells. To this end, Figure 3a compares the dipole moment distributions associated with water molecules residing within the first and second solvation shells of each alkali metal ion and the corresponding distribution calculated for water molecules in the bulk. This analysis shows that Li^+, with its high charge density and small size, significantly increases the dipole moment by about 10% for water molecules in the first shell compared to bulk water. As the ion size increases, from Li^+ to Cs^+, the dipole moment of the water molecules lying within the first solvation shells decreases, with the water molecules around the largest ions, Rb^+ and Cs^+, exhibiting dipole moments that are ∼2% smaller than that of bulk water. Figure 3b demonstrates that the effects of all alkali metal ions on the dipole moment of the surrounding water molecules is quite local; water molecules further out in the second shell display dipole moments similar to those in the bulk water, regardless of the ion present in solution. Interestingly, the present MB-nrg simulations predict that Na^+ does not affect the dipole moment of the water molecules, independently of the solvation shell they occupy. This

observation might explain why several models that assume a simple additive effect between ions and water can still reasonably predict the behavior of Na^+ in solution since Na^+ is the ion that changes the properties of the surrounding water the least. The lack of variation of the dipole moment for water molecules around Na^+ also suggests that using Na^+ as a benchmark for testing the accuracy of ion–water models might not be the best approach to the validation of these models since Na^+ alters the water properties only minimally. Similar local effects on the hydration properties of aqueous alkali halide solutions were observed in AIMD simulations using the PBE functional for NaCl,[104] as well as in MD simulations utilizing

a)

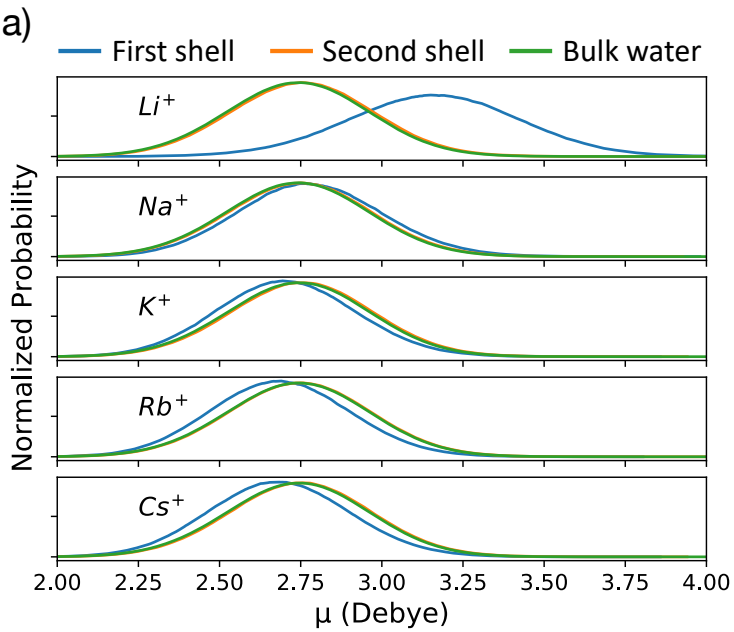

b)

	Li^+	Na^+	K^+	Rb^+	Cs^+
first shell	3.16	2.78	2.71	2.69	2.68
second shell	2.75	2.75	2.75	2.75	2.75
bulk water	2.74	2.74	2.74	2.74	2.74

Figure 3: a) Dipole moment distributions for water molecules located in the first and second solvation shells around each alkali metal ions as well as in bulk water. b) Average dipole moment (in Debye) of water molecules located in the first and second solvation shells around each alkali metal ion as well as in bulk water.

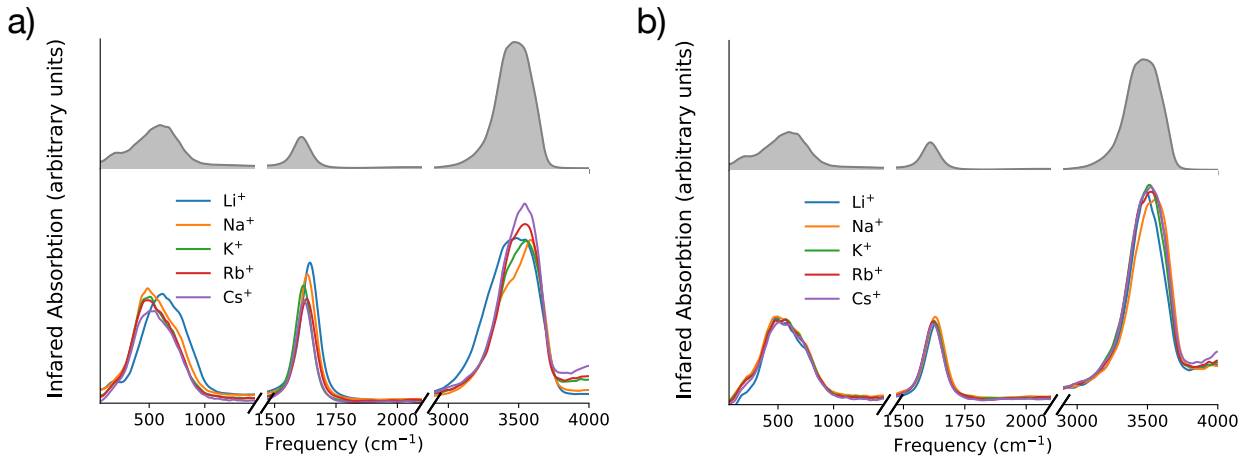

Figure 4: Infrared spectra calculated for water molecules located in the first (a) and second (b) solvation shells of each alkali metal ion. All spectra are redshifted by 60 cm^{-1} and 175 cm^{-1} in the bending and stretching regions, respectively, to account for nuclear quantum effects in classical MD simulations of vibrational spectra of water calculated with MB-pol as discussed in Refs. 53–55,78. The top trace corresponds to the infrared spectrum of liquid water calculated with MB-pol at 298 K.[55]

deep neural network potentials trained on SCAN and revPBE-D3 reference data for NaCl, KCl, and NaBr,[105] and NaCl and CsI,[106] respectively. These similarities, however, should be considered cautiously. Given the known functional-driven and density-driven errors in GGA and meta-GGA functionals[98,100,101] as well as the limitations of deep neural network potentials,[107,108] which prevent these models from correctly reproducing many-body interactions in aqueous systems,[35–38] it remains unclear if the locality observed in these simulations arises from the same physical mechanisms as those predicted by the present simulations with the MB-nrg potentials.

It should be noted that previous AIMD simulations reported slightly smaller dipole moments for water molecules residing within the first solvation shells of Na^+ and K^+ than in bulk.[30] The present MB-nrg simulations refine and extend the predictions from those AIMD simulations, showing that Na^+ does not modify the dipole moment of the surrounding water molecules, while Rb^+ and Cs^+ induce the larger reduction to the dipole moment of water molecules in their first solvation shells.

Figure 4 displays how the specific arrangement of water molecules around different alkali

metal ions and their varying dipole moments distinctly alter the IR spectra of the surrounding water molecules. In particular, independently of the alkali metal ion, the IR spectra change significantly from the first (panel a) to the second (panel b) solvation shells. As discussed above, due to its high charge density and small size, Li^+ induces a notable increase in the dipole moment of the water molecules that reside within the first solvation shell. These highly polarized water molecules thus form relatively stronger hydrogen bonds with water molecules in the second solvation shell, leading to a pronounced redshift in the OH-stretch band and a consequent blueshift in the HOH-bend band of the IR spectrum. Moreover, the wider OH-stretch band resulting from water molecules in the first solvation shell of Li^+ indicates a relatively larger distribution of hydrogen-bond strengths compared to the other alkali metal ions, reflecting a more inhomogeneous local environment.

As the ion's size increases, the IR spectral bands gradually shift. The shifts in the OH-stretch and HOH-bend bands for the larger alkali metal ions slowly approach the frequencies typical for bulk water, indicating a lesser impact on the water molecules' dipole moments. Figure 4b effectively confirms the predictions based on the variation of water's dipole moment as a function of the ion–water distance. The spectral differences seen in the IR spectra calculated for water molecules residing within the first solvation shell of each alkali-metal ion are no longer present in the second shell. The variation of the IR spectra from the first to the second solvation shells provides further support to the notion that the impact of the alkali metal ions on the hydrogen-bond network established by the surrounding water molecules is quite local, with water molecules beyond the first shell displaying similar behavior to those in bulk water.

CONCLUSIONS

In this study, we systematically examined the hydration structure of alkali metal ions (Li^+, Na^+, K^+, Rb^+, and Cs^+) in water using MD simulations carried out with the MB-nrg PEFs.

Our analyses include radial distribution functions, coordination numbers, residence times, dipole moments, and infrared spectra, providing a comprehensive view of the ions' influence on the hydrogen-bond network established by the surrounding water molecules. We found that Li^+ significantly increases the dipole moment of the water molecules residing within its first solvation shell, while larger alkali metal ions (i.e., Rb^+ and Cs^+) have the opposite impact, slightly reducing the dipole moment of the water molecules in their first solvation shells compared to bulk water. The changes in the dipole moments were found to directly reflect in appreciable frequency shifts of the OH-stretch and HOH-bend bands of the corresponding IR spectra. Importantly, the distinct variations in dipole moments and IR spectra between the first and second solvation shells predicted by the MD simulations with the MB-nrg PEFs demonstrate that, independently of their size and, consequently, charge density, the influence of all alkali metal ions on the properties of the surrounding water molecules is local, not extending beyond the first solvation shell. The remarkable agreement with available experimental data for the position and size of the first solvation shell around alkali metal ions in solution, along with previous results for interaction energies, vibrational spectra, and isomeric equilibria in small alkali metal ion–water clusters,[40,65–67] and simulations of EXAFS spectra,[68,69] provides further evidence for the accuracy and predictive power of the MB-nrg PEFs, making them highly promising for realistic simulations of ionic aqueous systems across different thermodynamic conditions and environments.

ACKNOWLEDGEMENT

This research was supported by the National Science Foundation through grant no. 2102309. This research used Expanse at the San Diego Supercomputer Center (SDSC) through allocation CHE230053 from the Advanced Cyberinfrastructure Coordination Ecosystem: Services & Support (ACCESS) program, which is supported by National Science Foundation grants nos. 2138259, 2138286, 2138307, 2137603, and 2138296, as well as the Triton Shared Com-

puting Cluster (TSCC) at SDSC.

ASSOCIATED CONTENT

Data Availability Statement

Any data generated and analyzed in this study are available from the authors upon request. The MB-nrg PEFs used in this study are available in our open-access MBX software that can be downloaded from https://github.com/paesanilab/MBX.

Supporting Information

Brief overview of the MB-pol and MB-nrg PEFs and their applications in the context of state-of-the-art computer simulations of various aqueous systems.

References

(1) Marcus, Y. *Ions in Solution and their Solvation*; John Wiley & Sons, 2015.

(2) Jencks, W. P. General Acid-Base Catalysis of Complex Reactions in Water. *Chem. Rev.* **1972**, *72*, 705–718.

(3) Conway, B. E. Ionic Hydration in Chemistry and Biophysics. **1981**,

(4) Sigel, A.; Sigel, H.; Sigel, R. K. *The Alkali Metal Ions: Their Role for Life*; Springer, 2016; Vol. 16.

(5) Johnson, D. *Metals and Chemical Change*; The Royal Society of Chemistry, 1999; pp 154–159.

(6) Tarascon, J.-M.; Armand, M. Issues and Challenges Facing Rechargeable Lithium Batteries. *Nature* **2001**, *414*, 359–367.

(7) Morth, J. P.; Pedersen, B. P.; Toustrup-Jensen, M. S.; Sørensen, T. L.-M.; Petersen, J.; Andersen, J. P.; Vilsen, B.; Nissen, P. Crystal Structure of the Sodium–Potassium Pump. *Nature* **2007**, *450*, 1043–1049.

(8) Atwood, D. A. *Radionuclides in the Environment*; John Wiley & Sons, 2013.

(9) Hofmeister, F. Zur Lehre von der Wirkung der Salze: Zzweite Mittheilung. *Arch. Exp. Pathol. Pharmacol.* **1888**, *24*, 247–260.

(10) Hofmeister, F. Zur Lehre von der Wirkung der Salze: Dritte Mittheilung. *Arch. Exp. Pathol. Pharmacol.* **1888**, *25*, 1–30.

(11) Gurney, R. W. *Ionic processes in solution*; McGraw-Hill, New York, 1953.

(12) Marcus, Y. Effect of Ions on the Structure of Water: Structure Making and Breaking. *Chem. Rev.* **2009**, *109*, 1346–1370.

(13) Selinger, A.; Castleman Jr, A. Evidence for the Encagement of Alkali Metal Ions through the Formation of Gas-Phase Clathrates: Cs^+ in Water Clusters. *J. Phys. Chem.* **1991**, *95*, 8442–8444.

(14) Beck, J. P.; Lisy, J. M. Infrared Spectroscopy of Hydrated Alkali Metal Cations: Evidence of Multiple Photon Absorption. *J. Chem. Phys.* **2011**, *135*, 044302.

(15) Cooper, R. J.; Chang, T. M.; Williams, E. R. Hydrated Alkali Metal Ions: Spectroscopic Evidence for Clathrates. *J. Phys. Chem. A* **2013**, *117*, 6571–6579.

(16) Buchner, R.; Wachter, W.; Hefter, G. Systematic Variations of Ion Hydration in Aqueous Alkali Metal Fluoride Solutions. *J. Phys. Chem. B* **2019**, *123*, 10868–10876.

(17) Mahler, J.; Persson, I. A Study of the Hydration of the Alkali Metal Ions in Aqueous Solution. *Inorg. Chem.* **2012**, *51*, 425–438.

(18) Giammanco, C. H.; Wong, D. B.; Fayer, M. D. Water Dynamics in Divalent and Monovalent Concentrated Salt Solutions. *J. Phys. Chem. B* **2012**, *116*, 13781–13792.

(19) Perrine, K. A.; Parry, K. M.; Stern, A. C.; Van Spyk, M. H.; Makowski, M. J.; Freites, J. A.; Winter, B.; Tobias, D. J.; Hemminger, J. C. Specific Cation Effects at Aqueous Solution– Vapor Interfaces: Surfactant-Like Behavior of Li^+ Revealed by Experiments and Simulations. *Proc. Natl. Acad. Sci. U.S.A.* **2017**, *114*, 13363–13368.

(20) Perera, L.; Berkowitz, M. L. Many-Body Effects in Molecular Dynamics Simulations of $Na^+(H_2O)_n$ and $Cl^-(H_2O)_n$ Clusters. *J. Chem. Phys.* **1991**, *95*, 1954–1963.

(21) Joung, I. S.; Cheatham III, T. E. Determination of Alkali and Halide Monovalent Ion Parameters for Use in Explicitly Solvated Biomolecular Simulations. *J. Phys. Chem. B* **2008**, *112*, 9020–9041.

(22) Sengupta, A.; Li, Z.; Song, L. F.; Li, P.; Merz Jr, K. M. Parameterization of Monovalent Ions for the OPC3, OPC, TIP3P-FB, and TIP4P-FB Water Models. *J. Chem. Inf. Model.* **2021**, *61*, 869–880.

(23) Zeron, I.; Abascal, J.; Vega, C. A Force Field of Li^+, Na^+, K^+, Mg^{2+}, Ca^{2+}, Cl^-, and SO_4^{2-} in Aqueous Solution Based on the TIP4P/2005 Water Model and Scaled Charges for the Ions. *J. Chem. Phys.* **2019**, *151*, 134504.

(24) Blazquez, S.; Conde, M.; Abascal, J.; Vega, C. The Madrid-2019 Force Field for Electrolytes in Water Using TIP4P/2005 and Scaled Charges: Extension to the Ions F^-, Br^-, I^-, Rb^+, and Cs^+. *J. Chem. Phys.* **2022**, *156*, 044505.

(25) Blazquez, S.; Conde, M.; Vega, C. Scaled Charges for Ions: An Improvement but Not the Final Word for Modeling Electrolytes in Water. *J. Chem. Phys.* **2023**, *158*, 054505.

(26) Dang, L. X.; Schenter, G. K.; Glezakou, V.-A.; Fulton, J. L. Molecular Simulation Analysis and X-ray Absorption Measurement of Ca^{2+}, K^+ and Cl^- Ions in Solution. *J. Phys. Chem. B* **2006**, *110*, 23644–23654.

(27) Jing, Z.; Liu, C.; Ren, P. Advanced Electrostatic Model for Monovalent Ions Based on Ab Initio Energy Decomposition. *J. Chem. Inf. Model.* **2021**, *61*, 2806–2817.

(28) Krekeler, C.; Hess, B.; Delle Site, L. Density Functional Study of Ion Hydration for the Alkali Metal Ions (Li^+, Na^+, K^+) and the halide ions (F^-, Br^-, Cl^-). *J. Chem. Phys.* **2006**, *125*, 054305.

(29) Varma, S.; Rempe, S. B. Coordination Numbers of Alkali Metal Ions in Aqueous Solutions. *Biophys. Chem.* **2006**, *124*, 192–199.

(30) Ikeda, T.; Boero, M.; Terakura, K. Hydration of Alkali Ions from First Principles Molecular Dynamics Revisited. *J. Chem. Phys.* **2007**, *126*, 034501.

(31) Bankura, A.; Carnevale, V.; Klein, M. L. Hydration Structure of Na^+ and K^+ from Ab Initio Molecular Dynamics Based on Modern Density Functional Theory. *Mol. Phys.* **2014**, *112*, 1448–1456.

(32) Ikeda, T.; Boero, M. Role of Van der Waals Corrections in First Principles Simulations of Alkali Metal Ions in Aqueous Solutions. *J. Chem. Phys.* **2015**, *143*.

(33) Galib, M.; Baer, M.; Skinner, L.; Mundy, C.; Huthwelker, T.; Schenter, G.; Benmore, C.; Govind, N.; Fulton, J. L. Revisiting the Hydration Structure of Aqueous Na^+. *J. Chem. Phys.* **2017**, *146*, 084504.

(34) Duignan, T. T.; Schenter, G. K.; Fulton, J. L.; Huthwelker, T.; Balasubramanian, M.; Galib, M.; Baer, M. D.; Wilhelm, J.; Hutter, J.; Del Ben, M. et al. Quantifying the Hydration Structure of Sodium and Potassium Ions: Taking Additional Steps on Jacob's Ladder. *Phys. Chem. Chem. Phys.* **2020**, *22*, 10641–10652.

(35) Sharkas, K.; Wagle, K.; Santra, B.; Akter, S.; Zope, R. R.; Baruah, T.; Jackson, K. A.; Perdew, J. P.; Peralta, J. E. Self-Interaction Error Overbinds Water Clusters dut Cancels in Structural Energy Differences. *Proc. Natl. Acad. Sci. U.S.A.* **2020**, *117*, 11283–11288.

(36) Dasgupta, S.; Lambros, E.; Perdew, J. P.; Paesani, F. Elevating Density Functional Theory to Chemical Accuracy for Water Simulations through a Density-Corrected Many-Body Formalism. *Nat. Commun.* **2021**, *12*, 1–12.

(37) Palos, E.; Lambros, E.; Swee, S.; Hu, J.; Dasgupta, S.; Paesani, F. Assessing the Interplay Between Functional-Driven and Density-Driven Errors in DFT Models of Water. *J. Chem. Theory Comput.* **2022**, *18*, 3410–3426.

(38) Dasgupta, S.; Shahi, C.; Bhetwal, P.; Perdew, J. P.; Paesani, F. How Good Is the Density-Corrected SCAN Functional for Neutral and Ionic Aqueous Systems, and What Is So Right About the Hartree–Fock Density? *J. Chem. Theory Comput.* **2022**, *18*, 4745–4761.

(39) Bajaj, P.; Götz, A. W.; Paesani, F. Toward Chemical Accuracy in the Description of Ion–Water Interactions through Many-Body Representations. I. Halide–Water Dimer Potential Energy Surfaces. *J. Chem. Theory Comput.* **2016**, *12*, 2698–2705.

(40) Riera, M.; Mardirossian, N.; Bajaj, P.; Götz, A. W.; Paesani, F. Toward Chemical Accuracy in the Description of Ion–Water Interactions through Many-Body Representations. Alkali-Water Dimer Potential Energy Surfaces. *J. Chem. Phys.* **2017**, *147*, 161715.

(41) Riera, M.; Yeh, E. P.; Paesani, F. Data-Driven Many-Body Models for Molecular Fluids: CO_2/H_2O Mixtures as a Case Study. *J. Chem. Theory Comput.* **2020**, *16*, 2246–2257.

(42) Riera, M.; Hirales, A.; Ghosh, R.; Paesani, F. Data-Driven Many-Body Models with Chemical Accuracy for CH_4/H_2O Mixtures. *J. Chem. Phys. B* **2020**, *124*, 11207–11221.

(43) Bull-Vulpe, E. F.; Riera, M.; Bore, S. L.; Paesani, F. Data-Driven Many-Body Potential Energy Functions for Generic Molecules: Linear Alkanes as a Proof-of-Concept Application. *J. Chem. Theory Comput.* **2023**, *19*, 4494–4509.

(44) Babin, V.; Leforestier, C.; Paesani, F. Development of a "First Principles" Water Potential with Flexible Monomers: Dimer Potential Energy Surface, VRT Spectrum, and Second Virial Coefficient. *J. Chem. Theory Comput.* **2013**, *9*, 5395–5403.

(45) Babin, V.; Medders, G. R.; Paesani, F. Development of a "First Principles" Water Potential with Flexible monomers. II: Trimer Potential Energy Surface, Third Virial Coefficient, and Small Clusters. *J. Chem. Theory Comput.* **2014**, *10*, 1599–1607.

(46) Medders, G. R.; Babin, V.; Paesani, F. Development of a "First-Principles" Water Potential with Flexible Monomers. III. Liquid Phase Properties. *J. Chem. Theory Comput.* **2014**, *10*, 2906–2910.

(47) Reddy, S. K.; Straight, S. C.; Bajaj, P.; Huy Pham, C.; Riera, M.; Moberg, D. R.; Morales, M. A.; Knight, C.; Götz, A. W.; Paesani, F. On the Accuracy of the MB-pol Many-Body Potential for Water: Interaction Energies, Vibrational Frequencies, and Classical Thermodynamic and Dynamical Properties from Clusters to Liquid water and Ice. *J. Chem. Phys.* **2016**, *145*, 194504.

(48) Paesani, F. Getting the Right Answers for the Right Reasons: Toward Predictive Molecular Simulations of Water with Many-Body Potential Energy Functions. *Acc. Chem. Res.* **2016**, *49*, 1844–1851.

(49) Bore, S. L.; Paesani, F. Realistic Phase Diagram of Water from "First Principles" Data-Driven Quantum Simulations. *Nat. Commun.* **2023**, *14*, 3349.

(50) Richardson, J. O.; Pérez, C.; Lobsiger, S.; Reid, A. A.; Temelso, B.; Shields, G. C.; Kisiel, Z.; Wales, D. J.; Pate, B. H.; Althorpe, S. C. Concerted Hydrogen-Bond Breaking by Quantum Tunneling in the Water Hexamer Prism. *Science* **2016**, *351*, 1310–1313.

(51) Cole, W. T.; Farrell, J. D.; Wales, D. J.; Saykally, R. J. Structure and Torsional Dynamics of the Water Octamer from THz Laser Spectroscopy Near 215 μm. *Science* **2016**, *352*, 1194–1197.

(52) Brown, S. E.; Götz, A. W.; Cheng, X.; Steele, R. P.; Mandelshtam, V. A.; Paesani, F. Monitoring Water Clusters "melt" through Vibrational Spectroscopy. *J. Am. Chem. Soc.* **2017**, *139*, 7082–7088.

(53) Medders, G. R.; Paesani, F. Infrared and Raman Spectroscopy of Liquid Water through "First-Principles" Many-Body Molecular Dynamics. *J. Chem. Theory Comput.* **2015**, *11*, 1145–1154.

(54) Medders, G. R.; Paesani, F. Dissecting the Molecular Structure of the Air/Water Interface from Quantum Simulations of the Sum-Frequency Generation Spectrum. *J. Am. Chem. Soc.* **2016**, *138*, 3912–3919.

(55) Reddy, S. K.; Moberg, D. R.; Straight, S. C.; Paesani, F. Temperature-Dependent Vibrational Spectra and Structure of Liquid Water from Classical and Quantum Simulations With the MB-pol Potential Energy Function. *J. Chem. Phys.* **2017**, *147*, 244504.

(56) Moberg, D. R.; Straight, S. C.; Paesani, F. Temperature Dependence of the Air/Water Interface Revealed by Polarization Sensitive Sum-Frequency Generation Spectroscopy. *J. Phys. Chem. B* **2018**, *122*, 4356–4365.

(57) Muniz, M. C.; Gartner III, T. E.; Riera, M.; Knight, C.; Yue, S.; Paesani, F.; Pana-

giotopoulos, A. Z. Vapor-Liquid Equilibrium of Water with the MB-pol Many-Body Potential. *J. Chem. Phys.* **2021**, *154*, 211103.

(58) Gartner III, T. E.; Hunter, K. M.; Lambros, E.; Caruso, A.; Riera, M.; Medders, G. R.; Panagiotopoulos, A. Z.; Debenedetti, P. G.; Paesani, F. Anomalies and Local Structure of Liquid Water from Boiling to the Supercooled Regime as Predicted by the Many-Body MB-pol Model. *J. Phys. Chem. Lett.* **2022**, *13*, 3652–3658.

(59) Pham, C. H.; Reddy, S. K.; Chen, K.; Knight, C.; Paesani, F. Many-Body Interactions in Ice. *J. Chem. Theory Comput.* **2017**, *13*, 1778–1784.

(60) Moberg, D. R.; Straight, S. C.; Knight, C.; Paesani, F. Molecular Origin of the Vibrational Structure of Ice I_h. *J. Phys. Chem. Lett.* **2017**, *8*, 2579–2583.

(61) Moberg, D. R.; Sharp, P. J.; Paesani, F. Molecular-Level Interpretation of Vibrational Spectra of Ordered Ice Phases. *J. Phys. Chem. B* **2018**, *122*, 10572–10581.

(62) Moberg, D. R.; Becker, D.; Dierking, C. W.; Zurheide, F.; Bandow, B.; Buck, U.; Hudait, A.; Molinero, V.; Paesani, F.; Zeuch, T. The End of Ice I. *Proc. Natl. Acad. Sci. U.S.A.* **2019**, *116*, 24413–24419.

(63) Stanton, J. F. Why CCSD(T) Works: A Different Perspective. *Chem. Phys. Lett.* **1997**, *281*, 130–134.

(64) Rezac, J.; Hobza, P. Benchmark Calculations of Interaction Energies in Noncovalent Complexes and Their Applications. *Chem. Rev.* **2016**, *116*, 5038–5071.

(65) Egan, C. K.; Bizzarro, B. B.; Riera, M.; Paesani, F. Nature of Alkali Ion–Water Interactions: Insights From Many-Body Representations and Density Functional Theory. II. *J. Chem. Theory Comput.* **2020**, *16*, 3055–3072.

(66) Riera, M.; Brown, S. E.; Paesani, F. Isomeric Equilibria, Nuclear Quantum Effects,

and Vibrational Spectra of $M^+(H_2O)_{n=1-3}$ Clusters, with M = Li, Na, K, Rb, and Cs, through Many-Body Representations. *J. Phys. Chem. A* **2018**, *122*, 5811–5821.

(67) Riera, M.; Talbot, J. J.; Steele, R. P.; Paesani, F. Infrared Signatures of Isomer Selectivity and Symmetry Breaking in the $Cs^+(H_2O)_3$ Complex Using Many-Body Potential Energy Functions. *J. Chem. Phys.* **2020**, *153*, 044306.

(68) Zhuang, D.; Riera, M.; Zhou, R.; Deary, A.; Paesani, F. Hydration Structure of Na^+ and K^+ Ions in Solution Predicted by Data-Driven Many-Body Potentials. *J. Phys. Chem. B* **2022**, *126*, 9349–9360.

(69) Zhuang, D.; Riera, M.; Schenter, G. K.; Fulton, J. L.; Paesani, F. Many-Body Effects Determine the Local Hydration Structure of Cs^+ in Solution. *J. Phys. Chem. Lett.* **2019**, *10*, 406–412.

(70) Thompson, A. P.; Aktulga, H. M.; Berger, R.; Bolintineanu, D. S.; Brown, W. M.; Crozier, P. S.; in 't Veld, P. J.; Kohlmeyer, A.; Moore, S. G.; Nguyen, T. D. et al. LAMMPS – A Flexible Simulation Tool for Particle-based Materials Modeling at the Atomic, Meso, and Continuum Scales. *Comput. Phys. Commun.* **2022**, *271*, 108171.

(71) Riera, M.; Knight, C.; Bull-Vulpe, E. F.; Zhu, X.; Agnew, H.; Smith, D. G. A.; Simmonett, A. C.; Paesani, F. MBX: A Many-Body Energy and Force Calculator for Data-Driven Many-Body Simulations. *J. Chem. Phys.* **2023**, *159*, 054802.

(72) MBX v1.0. `http://paesanigroup.ucsd.edu/software/mbx.html`, 2023.

(73) Martyna, G. J.; Klein, M. L.; Tuckerman, M. Nosé–Hoover Chains: The Canonical Ensemble Via Continuous Dynamics. *J. Chem. Phys.* **1992**, *97*, 2635–2643.

(74) Shinoda, W.; Shiga, M.; Mikami, M. Rapid Estimation of Elastic Constants by Molecular Dynamics Simulation under Constant Stress. *Phys. Rev. B* **2004**, *69*, 134103.

(75) Simmonett, A. C.; Brooks, B. R. Analytical Hessians for Ewald and Particle Mesh Ewald Electrostatics. *J. Chem. Phys.* **2021**, *154*, 104101.

(76) Simmonett, A. C.; Brooks, B. R. A Compression Strategy for Particle Mesh Ewald Theory. *J. Chem. Phys.* **2021**, *154*, 054112.

(77) Medders, G. R.; Paesani, F. Many-Body Convergence of the Electrostatic Properties of Water. *J. Chem. Theory Comput.* **2013**, *9*, 4844–4852.

(78) Hunter, K. M.; Shakib, F. A.; Paesani, F. Disentangling Coupling Effects in the Infrared Spectra of Liquid Water. *J. Phys. Chem. B* **2018**, *122*, 10754–10761.

(79) Rieth, A. J.; Hunter, K. M.; Dincă, M.; Paesani, F. Hydrogen Bonding Structure of Confined Water Templated by a Metal-Organic Framework With Open Metal Sites. *Nat. Commun.* **2019**, *10*, 1–7.

(80) Ho, C.-H.; Valentine, M. L.; Chen, Z.; Xie, H.; Farha, O.; Xiong, W.; Paesani, F. Structure and Thermodynamics of Water Adsorption in NU-1500-Cr. *Commun. Chem* **2023**, *6*, 70.

(81) Medders, G. R.; Paesani, F. On the Interplay of the Potential Energy and Dipole Moment Surfaces in Controlling the Infrared Activity of Liquid Water. *J. Chem. Phys.* **2015**, *142*, 212411.

(82) Straight, S. C.; Paesani, F. Exploring Electrostatic Effects on the Hydrogen Bond Network of Liquid Water through Many-Body Molecular Dynamics. *J. Phys. Chem. B* **2016**, *120*, 8539–8546.

(83) Hudait, A.; Moberg, D. R.; Qiu, Y.; Odendahl, N.; Paesani, F.; Molinero, V. Preordering of Water Is Not Needed for Ice Recognition by Hyperactive Antifreeze Proteins. *Proc. Natl. Acad. Sci. U.S.A.* **2018**, *115*, 8266–8271.

(84) Reddy, S. K.; Thiraux, R.; Rudd, B. A. W.; Lin, L.; Adel, T.; Joutsuka, T.; Geiger, F. M.; Allen, H. C.; Morita, A.; Paesani, F. Bulk Contributions Modulate the Sum-Frequency Generation Spectra of Water on Model Sea-Spray Aerosols. *Chem* **2018**, *4*, 1629–1644.

(85) Hunter, K. M.; Wagner, J. C.; Kalaj, M.; Cohen, S. M.; Xiong, W.; Paesani, F. Simulation Meets Experiment: Unraveling the Properties of Water in Metal–Organic Frameworks Through Vibrational Spectroscopy. *J. Phys. Chem. C* **2021**, *125*, 12451–12460.

(86) Wagner, J. C.; Hunter, K. M.; Paesani, F.; Xiong, W. Water Capture Mechanisms at Zeolitic Imidazolate Framework Interfaces. *J. Am. Chem. Soc.* **2021**, *143*, 21189–21194.

(87) Cao, J.; Voth, G. A. The Formulation of Quantum Statistical Mechanics Based on the Feynman Path Centroid Density. I. Equilibrium Properties. *J. Chem. Phys* **1994**, *100*, 5093–5105.

(88) Cao, J.; Voth, G. A. The Formulation of Quantum Statistical Mechanics Based on the Feynman Path Centroid Density. II. Dynamical Properties. *J. Chemical Phys.* **1994**, *100*, 5106–5117.

(89) Cao, J.; Voth, G. A. The Formulation of Quantum Statistical Mechanics Based on the Feynman Path Centroid Density. III. Phase Space Formalism and Analysis of Centroid Molecular Dynamics. *J. Chem. Phys.* **1994**, *101*, 6157–6167.

(90) Cao, J.; Voth, G. A. The Formulation of Quantum Statistical Mechanics Based on the Feynman Path Centroid Density. IV. Algorithms for Centroid Molecular Dynamics. *J. Chem. Phys.* **1994**, *101*, 6168–6183.

(91) Cao, J.; Voth, G. A. The Formulation of Quantum Statistical Mechanics Based on the

Feynman Path Centroid Density. V. Quantum Instantaneous Normal Mode Theory of Liquids. *J. Chem. Phys.* **1994**, *101*, 6184–6192.

(92) Jang, S.; Voth, G. A. Path Integral Centroid Variables and the Formulation of Their Exact Real Time Dynamics. *J. Chem. Phys.* **1999**, *111*, 2357–2370.

(93) Jang, S.; Voth, G. A. A Derivation of Centroid Molecular Dynamics and Other Approximate Time Evolution Methods for Path Integral Centroid Variables. *J. Chem. Phys.* **1999**, *111*, 2371–2384.

(94) Impey, R.; Madden, P.; McDonald, I. Hydration and Mobility of Ions in Solution. *J. Phys. Chem.* **1983**, *87*, 5071–5083.

(95) Zhou, L., Qian Quantifying the Structure of Water and Hydrated Monovalent Ions by Density Functional Theory-Based Molecular Dynamics. *J. Phys. Chem. B* **2022**, *126*, 10471–10480.

(96) Paesani, F.; Bajaj, P.; Riera, M. Chemical Accuracy in Modeling Halide Ion Hydration from Many-Body Representations. *Adv. Phys. X* **2019**, *4*, 1631212.

(97) Bizzarro, B. B.; Egan, C. K.; Paesani, F. Nature of Halide–Water Interactions: Insights From Many-Body Representations and Density Functional Theory. *J. Chem. Theory Comput.* **2019**, *15*, 2983–2995.

(98) Vuckovic, S.; Song, S.; Kozlowski, J.; Sim, E.; Burke, K. Density Functional Analysis: The Theory of Density-Corrected DFT. *J. Chem. Theory Comput.* **2019**, *15*, 6636–6646.

(99) Lambros, E.; Hu, J.; Paesani, F. Assessing the Accuracy of the SCAN Functional for Water Through a Many-Body Analysis of the Adiabatic Connection Formula. *J. Chem. Theory Comput.* **2021**, *17*, 3739–3749.

(100) Song, S.; Vuckovic, S.; Sim, E.; Burke, K. Density-Corrected DFT Explained: Questions and Answers. *J. Chem. Theory Comput.* **2022**, *18*, 817–827.

(101) Sim, E.; Song, S.; Vuckovic, S.; Burke, K. Improving Results by Improving Densities: Density-Corrected Density Functional Theory. *J. Am. Chem. Soc.* **2022**, *144*, 6625–6639.

(102) Belleflamme, F.; Hutter, J. Radicals in Aqueous Solution: Assessment of Density-Corrected SCAN Functional. *Phys. Chem. Chem. Phys.* **2023**, *25*, 20817–20836.

(103) Palos, E.; Caruso, A.; Paesani, F. Consistent Density Functional Theory-Based Description of Ion Hydration Through Density-Corrected Many-Body Representations. *J. Chem. Phys.* **2023**, *159*, 181101.

(104) Gaiduk, A. P.; Galli, G. Local and Global Effects of Dissolved Sodium Chloride on the Structure of Water. *J. Phys. Chem. Lett.* **2017**, *8*, 1496–1502.

(105) Zhang, C.; Yue, S.; Panagiotopoulos, A. Z.; Klein, M. L.; Wu, X. Dissolving Salt Is Not Equivalent to Applying a Pressure on Water. *Nat. Commun.* **2022**, *13*, 822.

(106) Avula, N. V.; Klein, M. L.; Balasubramanian, S. Understanding the Anomalous Diffusion of Water in Aqueous Electrolytes Using Machine Learned Potentials. *J. Phys. Chem. Lett.* **2023**, *14*, 9500–9507.

(107) Gao, A.; Remsing, R. C. Self-Consistent Determination of Long-Range Electrostatics in Neural Network Potentials. *Nat. Commun.* **2022**, *13*, 1572.

(108) Zhai, Y.; Caruso, A.; Bore, S. L.; Luo, Z.; Paesani, F. A "Short Blanket" Dilemma for a State-of-the-Art Neural Network Potential for Water: Reproducing Experimental Properties or the Physics of the Underlying Many-Body Interactions? *J. Chem. Phys.* **2023**, *158*, 084111.

TOC Graphic

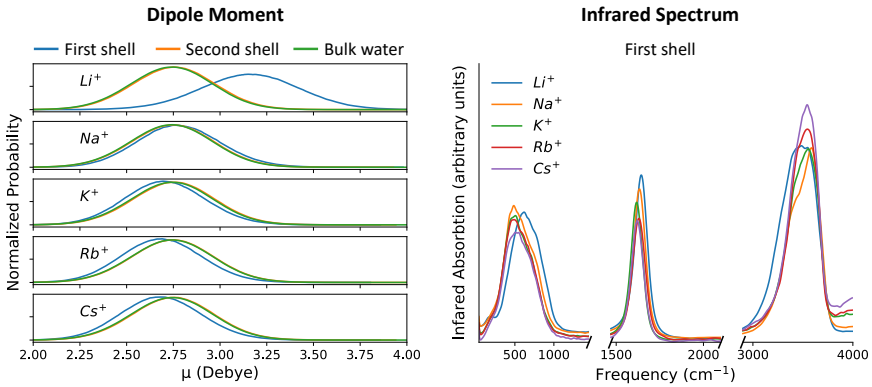
Dipole Moment
First shell
Second shell
Bulk water
Li^+
Na^+
K^+
Rb^+
Cs^+
Normalized Probability
2.00
2.25
2.50
2.75
3.00
3.25
3.50
3.75
4.00
μ (Debye)
Infrared Spectrum
First shell
Li^+
Na^+
K^+
Rb^+
Cs^+
Infared Absorbtion (arbitrary units)
500
1000
1500
2000
3000
4000
Frequency (cm^{-1})